ESPL WILEY

When do rock glacier fronts fail? Insights from two case studies in South Tyrol (Italian Alps)

Christian Kofler[1,2] | Volkmar Mair[3] | Stephan Gruber[4] |
Maria Cristina Todisco[5] | Ian Nettleton[5] | Stefan Steger[1] | Marc Zebisch[1] |
Stefan Schneiderbauer[1,6,7] | Francesco Comiti[2]

[1]Institute for Earth Observation, Eurac Research, Bozen/Bolzano, Italy

[2]Faculty of Science and Technology, Free University of Bozen-Bolzano, Bozen/Bolzano, Italy

[3]Office for Geology and Building Materials Testing, Autonomous Province of Bozen/Bolzano, Kardaun-Cardano, Italy

[4]Department of Geography and Environmental Studies, Carleton University, Ottawa, Canada

[5]Coffey Geotechnics Ltd, Manchester, UK

[6]Institute for Environment and Human Security, GLOMOS Programme, United Nations University, Italy-Bozen/Bolzano-Bonn, Germany

[7]Department Geography, University of the Free State, Bloemfontein, South Africa

Correspondence
Christian Kofler, Institute for Earth Observation, Eurac Research, Drusuallee 1, 39100, Bozen/Bolzano, Italy.
Email: christiankofler@hotmail.com.

Funding information
Stiftung Südtiroler Sparkasse / Fondazione Cassa di Risparmio di Bolzano; Eurac Research

Abstract

The fronts of two rock glaciers located in South Tyrol (Italian Alps) failed on 13 August 2014, initiating debris flows in their downslope channels. A multimethod approach including climate, meteorological, and ground temperature data analysis, aerial image correlation, as well as geotechnical testing and modeling, led to the reconstruction of the two events. An integrated investigation of static predisposing factors, slowly changing preparatory factors, and potential triggering events shed light on the most likely reasons for such failures. Our results suggest that the occurrence of front destabilization at the two rock glaciers can only partly be explained by the occurrence of heavy rainfall events. Indeed, antecedent hydrological and thermal ground conditions were characterized by a saturated active layer favored by a snow-rich winter and extensive precipitation in late spring and summer. Also, the rising trend of air temperature during spring and summer months since 1950s might explain the concurrent marked displacement of the two rock glaciers. Indeed, geotechnical investigations have provided strong indications that one of the investigated rock glacier fronts was at a marginally stable state prior to 2014. As rainfall events more intense than the one that occurred in August 2014 were previously recorded in the same area without resulting failures at the studied rock glaciers, we propose that both predisposing and preparatory destabilizing factors have played a key role in the 2014 rock glacier front failures.

1 | INTRODUCTION

Climate change is strongly affecting the global cryosphere and leads to an increase in permafrost temperatures (IPCC, 2019). Permafrost influences livelihoods in Arctic and high mountain areas worldwide, and its thawing has already caused negative impacts in terms of an increased occurrence of geohazards and a deteriorating quality and supply of water (GAPHAZ, 2017; Hock et al., 2019; Jones et al., 2018; Schlögel et al., 2020; Thies et al., 2013). Although permafrost exists beneath larger areas than the area of glaciers in many countries, it has received substantially less attention mainly because it is a largely invisible phenomenon (Gruber et al., 2017). This may also explain why rock glaciers, one of the few landforms that testify to the presence of permafrost in mountain areas, increasingly came into

the spotlight of scientific research (Barsch, 1996; Berthling, 2011; Haeberli et al., 2006).

Although the effect of atmospheric warming on rock glaciers is not as immediate as on glaciers, they too are affected, as recent findings confirm (Delaloye et al., 2010; Jones et al., 2018). Observations show a link between long-term trends of permafrost temperatures and rock glacier displacement (PERMOS, 2019). Two internal processes determine the downslope movement of a rock glacier, namely plastic deformation of its frozen core and shearing along a distinct shear horizon (Buchli et al., 2018; Cicoira et al., 2019b; Kenner et al., 2017, 2019). Both processes are controlled by external environmental as well as internal, material-related parameters. The volumetric ice content and the temperature of the rock glacier material primarily control plastic deformation, while shearing deformation is mainly

driven by pore pressure induced by the presence of liquid water in the shear horizon (Arenson & Springman, 2005; Cicoira et al., 2019b). The presence of "warm" ice-rich material in rock glaciers therefore may translate into an acceleration of their displacement (Avian et al., 2009; Delaloye et al., 2013; Scotti et al., 2017; Vivero & Lambiel, 2019).

Mass wasting at rock glacier fronts mainly affects the unfrozen domain of the landform, but it should not be viewed as process disconnected from its internal ice-driven deformation. Due to the advancing of the rock glacier body, a creep pressure is induced to its front, causing an oversteepening and subsequent adjustment of the slope once a critical inclination is reached. In flat terrain, this continuous reworking of the front slope creates a layer of coarser sediment at the rock glacier's toe, which opposes the creep pressure through frictional resistance (Haeberli et al., 1998; Springman et al., 2012). If the terrain steepness at a rock glaciers toe favors the removal of such loose material, the latter may be transported downhill as debris flow, debris slide, or rock fall (Krainer et al., 2012; Kummert & Delaloye, 2018; Kummert et al., 2017; Lugon & Stoffel, 2010; Marcer et al., 2020).

Parts of the front slopes of two active rock glaciers—Hintergrat and Similaungrube—failed nearly simultaneously on 13 August 2014. The rock glaciers are about 50 km apart within the Vinschgau/ Venosta Valley (South Tyrol, northern Italy) (Figure 1). Both slope failures developed into debris flows that affected downstream infrastructure. Field visits were carried out immediately after the occurrence of the events and revealed exposed ice at the detachment scarps, indicating a role of permafrost degradation among the causing factors of the two detachments (Figure 2). Besides these two rock glacier front failures, 25 other events that required an intervention of civil protection authorities occurred on the same day, including debris flows, debris floods, and floods (Figure 1). Civil protection authorities identified glaciers to be the origin of at least three debris flows.

In this paper, we aim to identify the factors controlling rock glacier front stability, quantify their magnitude and put them into an Alpine-wide context, specifically addressing the two front failures that occurred in South Tyrol in 2014. Besides the short-term triggering rainfall event, we examine medium-term changes in climate and ground temperature variables, surface displacement rates, as well as static predisposing geotechnical and topographic characteristics of our study objects, and a reference site. A multimethod approach including aerial image correlation, material testing, and slope stability modeling, as well as borehole, precipitation, and climate data analysis supports the testing of hypotheses on slope failure mechanisms. These hypotheses are stated in section 3.1, after relevant details about the sites and events have been presented. Finally, an integrated view on rock glacier front stability is provided by comparing our results with findings on comparable sites in the European Alps.

2 | STUDY SITES

The present study was conducted in the Autonomous Province of Bolzano-Bozen (South Tyrol), a region located in the Eastern Italian Alps, bordering with Austria and Switzerland. The two rock glaciers affected by front failure—Hintergrat (HIN) and Similaungrube (SIM)— are located in the Vinschgau/Venosta Valley, which is located in the western part of the province (Figure 1). Both the rock glacier inventory by Bollmann et al. (2012) and the modeling results by Kofler et al. (2020) suggest the presence of permafrost ice in both studied rock glaciers. Figure 1 shows also the location of the near Lazaun rock glacier (LAZ), which served as reference site in this study. Ground temperature (GT, accuracy 0.1°C) was measured in this latter rock glacier in two 30- and 40-m-deep boreholes (Krainer et al., 2015).

2.1 | Hintergrat rock glacier (HIN)

This rock glacier lies on the eastern flank of Ortler/Ortles (3,905 m a.s.l.), South Tyrol's highest peak, located in the Sulden/Solda Valley, a lateral valley of the Vinschgau Valley. The rock glacier is oriented along a northeast–southwest extending crest adjacent to the Ende-der-Welt glacier, a glacier mostly covered by debris. The rock glacier setting is quite peculiar both in terms of topography and geology. Regarding the former, well-developed furrows and ridges on the upper part of the rock glacier indicate a flow line along the crest. The front is connected downslope to a steep channel, which makes HIN a type B rock glacier according to the classification of Kummert et al. (2017) (Figures 1 and 2). In terms of geology, HIN lies on two geological units, the Ortles nappe (dolomitic rocks) and the Campo nappe (metamorphic rocks) (Mair et al., 2007; Stingl & Mair, 2005). However, the sediment found within the rock glacier derives from the Ortles nappe only and consists partially of till (Table 1).

On 13 August 2014, during a rainfall event, a lateral part of the rock glacier front failed forming a debris flow in the Schrei creek channel. Within the channel, the debris flow entrained morainic and colluvial sediments and severely damaged hiking trails. The debris flow mostly deposited on the Schrei Creek fan, but part of the volume reached the Sulden/Solda River near the Village of Sulden (about 1,900 m a.s.l.). Post-event surveys were carried out by the local Civil Protection Agency and revealed a deposited volume of approximately 11,000 m^3, with boulders up to 3.5 m in diameter. Figure 2 shows the HIN rock glacier front with the clearly visible detachment scarp on the left side, where patches of clean ice are visible. Signs of erosion were visible at the failure zone on the eastern flank of the front slope prior to 2014. Apparently, water outflow at the rock glacier snout was concentrated at this pre-existing channel. The slope failure was followed by two minor events on 8 June 2015 and 12 July 2016.

2.2 | Similaungrube rock glacier (SIM)

The Similaungrube (SIM) rock glacier is located in a southwest-oriented cirque below the Similaun peak (3,599 m a.s.l.), which lies along the main Alpine ridgeline. Similarly to HIN, SIM is also a type B rock glacier, according to Kummert et al. (2017), as its front is connected to a steep channel (Figures 1 and 2). The rock glacier is mainly nourished by talus derived from the adjacent rock cliffs characterized by metamorphic rocks including schists belonging to the Ötztal-Stubai basement (Table 1). Morphologically, SIM features well-defined ridges and furrows.

On 13 August 2014, and nearly simultaneously with the triggering event at HIN, part of the SIM front slope failed. The detachment was clearly visible as a longitudinal scar in the front slope, about 190 m long
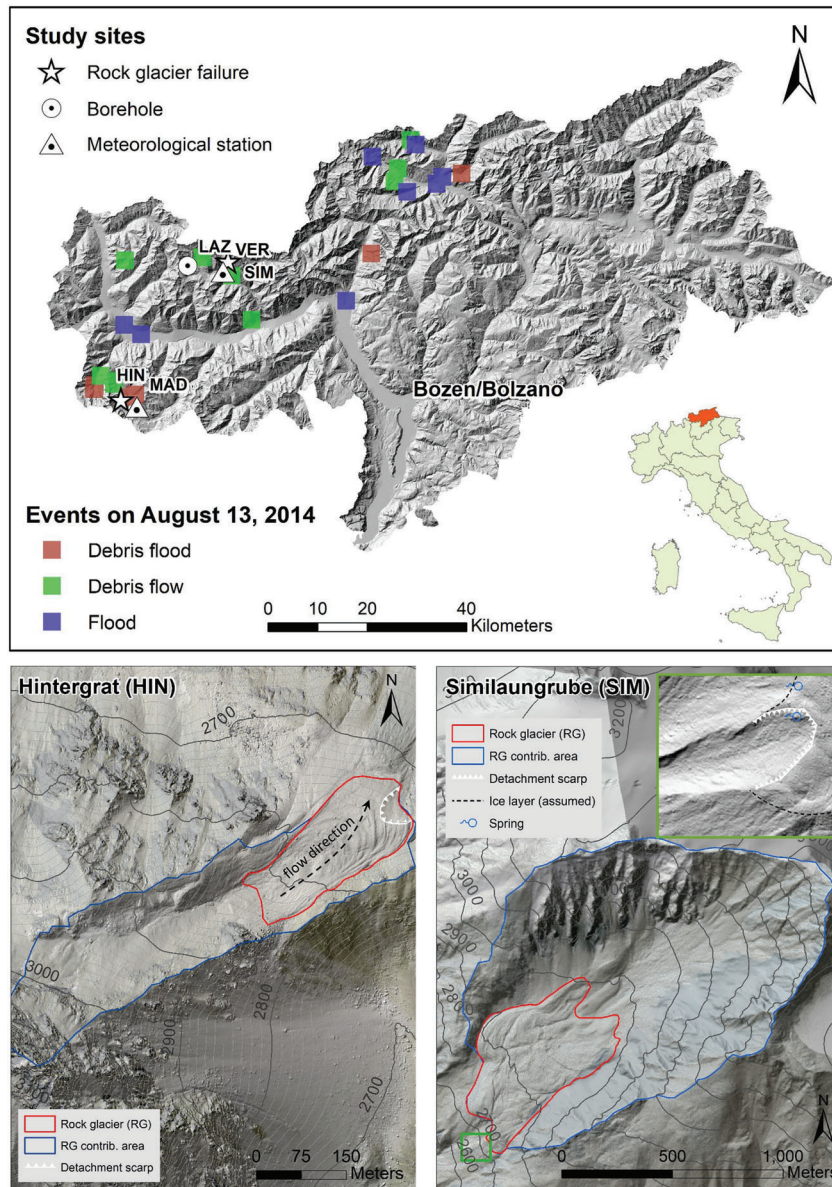
FIGURE 1 Regional context of study; location of failure sites, meteorological stations, borehole site, and registered hazard events on 31 August 2014 (upper panel). Detailed view of the failure sites HIN and SIM. Rock glacier outlines were taken over unchanged from the rock glacier inventory of Bollmann et al. (2012) (lower panel). Locations of rock glacier sites: 46° 30.469'N/10° 34.418'E (HIN), 46° 45.286'N/10° 51.645'E (SIM), 46° 44.826'N/10° 45.361'E (LAZ)

and 45 m wide. The detached material formed a debris flow along the Tisental Creek, eventually stopping into the Vernagt/Vernago hydropower reservoir. Image "SIM B" of Figure 2 was taken immediately after the failure event. Two layers of ice-rich debris are visible at the detachment scarp, and the ice-rich permafrost body below the debris mantle of the rock glacier can also be seen. While the failure zone of 2014 apparently was unaffected by previous detachments, scarps of smaller debris slides were visible on the northern part of the front. The only additional event present in the regional inventory of geo-hydrological hazards is a small debris flow on 29 July 2014.

3 | DATA AND METHODS

3.1 | Selection of destabilizing factors and development of hypotheses

A set of potentially destabilizing factors was identified based on previous findings in literature (see introduction). We differentiated

between temporally constant (*predisposing*), slowly changing (*preparatory*), and rapidly varying (*triggering*) destabilizing factors (Glade & Crozier, 2005; Steger, 2017). This concept was recently used to discuss causes for collapses of rock glaciers (Bodin et al., 2017) and their front slopes (Marcer et al., 2020) in the French Alps. Within the context of this approach, we aim to test three hypotheses on interactions of destabilizing factors:

Hypothesis 1: *Predisposing sedimentary composition and the triggering rainfall event were the causes for the failure events.*

Hypothesis 2: *Medium-term climatic and meteorological destabilizing preparatory factors affected the subsurface thermal and hydrological conditions of the study rock glaciers, in addition to the sedimentary composition and the triggering rainfall event.*

Hypothesis 3: *Rock glacier displacement over the previous years increased the predisposition to failure of the front slopes and acted together with the processes listed for hypothesis 2.*

FIGURE 2 Images of studied rock glacier (HIN for Hintergrat, SIM for Similaungrube) front failures: Two spring outlets are visible on the image "SIM B," one with visible water discharge on the detachment scarp above upper ice layer and a non-water carrying one further north. Photos "SIM A," "SIM B," and "HIN A" courtesy of the Autonomous Province of Bozen-Bolzano
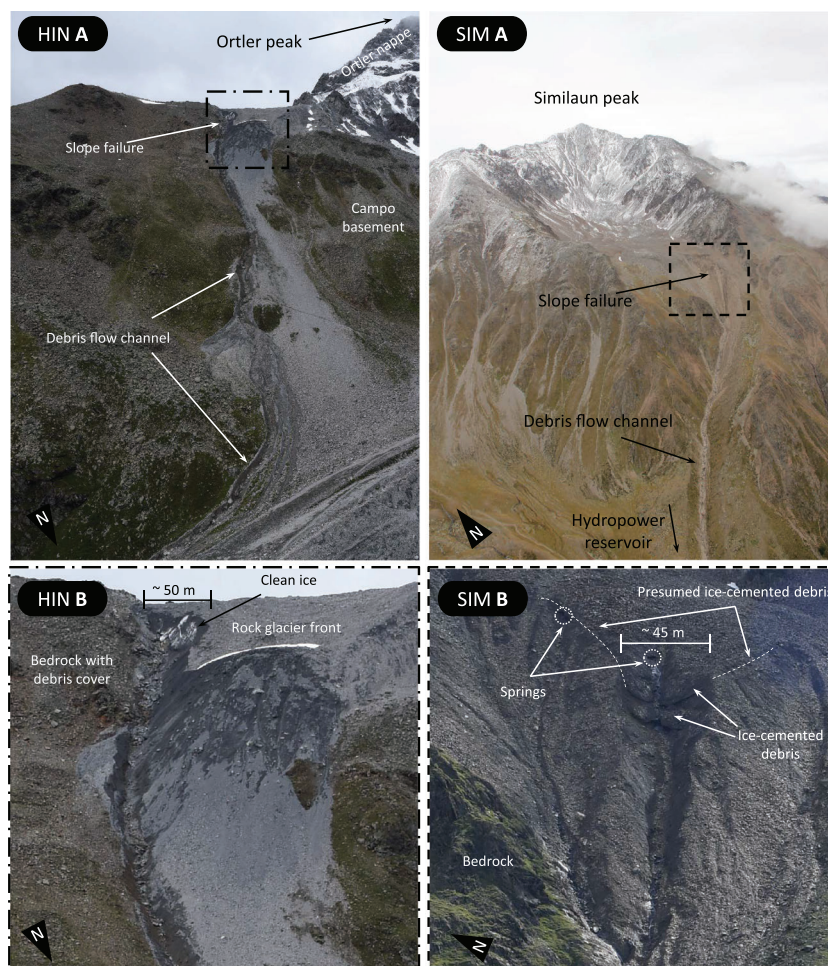

TABLE 1 Basic information regarding position, elevation, geometry, and bedrock geology of the two studied sites and their contributing areas

	HIN	SIM
Location	46° 30.469'N/10° 34.418'E	46° 45.286'N/10° 51.645'E
Front elevation [m a.s.l.]	2,700	2,750
Aspect [−]	NE	SW
Length [m]	290	780
Width [m]	145	400
Rock glacier area [m²]	33,300	282,400
Contributing area [m²]	117,400	1,633,200
Bedrock material [−]	Dolomite	Paragneiss

A geotechnical study including material testing and slope stability modeling as well as a reconstruction of rainfall conditions during the failure events were conducted to test hypothesis 1 (section 3.3.2 and 3.4). An analysis of ground temperature (GT) and key climate variables such as air temperature, precipitation and snow water equivalent (SWE) was carried out to test hypothesis 2 (section 3.3.1 and 3.5). Hypothesis 3 was tested by reconstructing surface movement of both sites based aerial image correlation (section 3.2).

3.2 | Rock glacier movement

Orthoimages were used to calculate horizontal movement of both studied rock glaciers over 14 years for HIN (2006–2019) and 15 years for SIM (2000–2014). The orthoimages taken in the years 2000, 2006, 2008, and 2014 are freely available on the WebGIS portal of the South Tyrolean provincial government[1]. The 2016 and 2019 products were instead taken during ad hoc photogrammetric and LiDAR (light detection and ranging) flights, respectively. Rock glacier movement was reconstructed by extracting 2D displacement vectors between image-pairs of orthoimages. The image-pairs were firstly manually co-registered in ArcGIS 10.7.1. The IMCORR algorithm (Bernstein, 1983), implemented in the open-source software package SAGA GIS 6.3.0 (Conrad et al., 2015), was deployed within the statistical computing software R (R Core Team, 2017). The RSAGA package (Brenning, 2008) was then used to compute surface displacement rates between two subsequent images. The threshold of detectable movement was identified by calculating the mean surface displacement rate within a manually mapped flat, presumably stable bedrock area. The obtained dataset was cleaned by removing vectors below the lower threshold of detection, over snow patches, shaded areas or those with an unlikely large displacement rate or direction (e.g., uphill). A mean annual displacement rate in m year⁻¹ was computed by averaging movement vectors for various sub-areas of HIN and SIM. A continuous dataset of absolute displacement rates and direction was created for each period by interpolating the relative variables using the "Ordinary Kriging"

algorithm, also available in SAGA GIS. The quality of each interpolated map was evaluated based on a k-fold cross validation (CV) and expressed in terms of a root mean square error (RMSE). Rock glacier movement and flow direction over the whole period were obtained by merging the gridded maps of the single periods.

3.3 | Climate and meteorological parameters

3.3.1 | Climate trends

Spatially interpolated datasets (250 m) of air temperature (T_A) and precipitation (P) at a monthly and daily temporal resolution based on the meteorological station network of South Tyrol and its neighboring regions were available for this study (Crespi et al., 2021). The gridded monthly datasets of T_A and P cover the periods 1956–2018 and 1950–2018, respectively. The daily datasets of both T_A and P range from 1980 to 2018. Time series of monthly and daily P and T_A values were extracted from the gridded datasets at the locations of HIN, SIM, and the nearby LAZ rock glacier (Figure 1). Snow water equivalent (SWE) was reconstructed for HIN, SIM, and LAZ with a degree-day model implemented in the hydrological modeling infrastructure GeoFrame (Formetta et al., 2011, 2014). Details about the modeling process can be found in the additional material and in Table S1-S3 and Figure S1.

A Mann–Kendall test was applied on seasonal aggregates of the monthly time series of T_A and P to study whether they have significantly changed since the 1950s (Kendall, 1957; Mann, 1945). The Theil–Sen estimator was used to compute the slope, that is, an annual change rate of the trend component (Sen, 1968; Theil, 1950). Derivatives of T_A, P, and SWE were computed to provide an enhanced comprehension of the climatic conditions that led to the failures. The positive degree day sum from the beginning of the year until the failure date (1 January to 13 August, PDD) for the daily time series 1980–2018 was computed for HIN and SIM to approximate the available energy for melting per year until the failure date (cf. Hartl et al., 2016). The cumulated precipitation for the months of June, July, and August (P_{JJA}) from 1950 to 2018 was computed to study the effect of liquid precipitation input during later spring and summer into the rock glacier system. The maximum SWE (SWE_{max}) for each winter season from 1980 to 2018 was extracted from the daily time series, beside the number of days until zero SWE (SWE_0) was reached. To approximate the intensity of melt water input, an average melting rate (MLT) in mm d^{-1} for the period between SWE_{max} and SWE_0 was computed.

3.3.2 | Rainfall depth and intensity prior to failure

Sub-hourly rainfall data was gathered from the meteorological stations Madritsch (MAD) and Vernagt (VER, Figure 1). Madritsch is the closest station to the HIN rock glacier (~3.5 km) and is located at 2,825 m a.s.l. About 2.6 km separates the SIM rock glacier from Vernagt, which is located at 1,700 m a.s.l. Both stations record precipitation at 5-min intervals. The continuous time series of precipitation records at both stations were discretized heuristically into single rainfall events. The criteria to separate two events were: (i) a cumulative amount of rainfall greater or equal to 0.5 mm and (ii) 6 h of rainfall smaller than 1 mm in between. Rainfall depth E (mm) and mean

intensity I (mm h^{-1}) were computed for each event and plotted against its duration D (h). A threshold separating the 50% and 95% cumulative frequency of all events was calculated with the frequentist approach presented by Brunetti et al. (2010). Existing intensity-duration (ID) and event-duration (ED) curves for debris flow initiation in South Tyrol and the neighboring province Trentino were shown for comparison (Marra et al., 2016; Nikolopoulos et al., 2015).

3.4 | Geomorphological and geotechnical characteristics

Geotechnical characteristics of the rock glacier fronts were studied to infer their stability. Sediment samples were taken at HIN (August 2018), SIM (September 2019), and LAZ (October 2018) to derive key geotechnical parameters such as grain size distribution (GSD), internal friction angle (φ), and apparent cohesion (c'). GSD of the coarse debris layer on top of the rock glaciers was obtained by performing in-situ grid counts (Bunte & Abt, 2001). Fine sediment was extracted from about 1-m-deep trenches dug at the front (HIN, SIM, and LAZ) and lateral (HIN and LAZ) slopes of the rock glaciers (Figure 6). After sieving, direct shear tests were conducted to determine c' and φ of the sediment samples (cf. Curry et al., 2009; Rathbun et al., 2008). Two tests were performed for each sample with a varying range of normal stresses (σ_N); during the first test the range of σ_N varied between 0 and 100 kPa, while during the second test σ_N varied between 45 and 200 kPa. The values for c' and φ were obtained by applying the Mohr–Coulomb failure criterion of linearity between σ_N and the measured peak shear strength τ_{max}.

To complement our set of geotechnical parameters, we firstly conducted a literature research on direct shear tests of material derived from glacial and periglacial landforms (moraines, rock glaciers, and scree slopes). Second, we performed a probabilistic back-analysis of the failure events (cf. Lacasse et al., 2017; Tang, 1984; Zhang et al., 2010). The sliding surface relative to the august 2014 events had to be reconstructed first. For this, we extracted a reference- and a post-failure cross section from a set of multitemporal digital surface models (DSMs) taken in 2006 and 2016. The former DSM derives from an airborne LiDAR survey of the entire province of South Tyrol, and features a geometric resolution of 2.5 m and a vertical accuracy of 0.55 m. The 2016 DSM was photogrammetrically generated over the glacial areas of South Tyrol and has a geometric resolution of 0.5 m and a vertical accuracy of 0.1 m. We computed a rock glacier thinning rate (m year^{-1}) by subtracting the 2006 DSM from the 2016 DSM for central areas of HIN and SIM (i.e., by excluding frontal and rooting zones) and dividing the elevation loss by the number of years (11) between the acquisition of the DSMs. The calculated annual thinning rate was then applied to the reference and post-failure cross section. Model parameters c', φ, and pore pressure were treated as random variables, characterized by a mean and standard deviation (e.g., Nadim, 2007).

Pore pressure was expressed as a fraction of vertical stress exerted by the soil column on the sliding plane and denoted as r_u (Bishop & Morgenstern, 1960; El-Ramly et al., 2005). Slope stability was computed through a 2D limit-equilibrium method available in the software package "Slide2" (Rocscience, 2019). Bishop's simplified method was applied to model the slope failure (Bishop, 1955). Random parameter sets (n = 1,000) were generated with a Latin hypercube sampler. A global minimum slip surface was identified firstly by a

deterministic slope stability analysis. Then, a probabilistic analysis was carried out on the global minimum slip surface, using the randomly generated parameter samples. Four model simulations featuring different configurations of c', φ, and r_u were performed to determine their relevance for the stability of the examined slopes:

1. A dry and cohesionless sediment characterized only by φ was modeled. We assumed φ to be normally distributed with its maximum measured value as mean.
2. An additional strength-component was included by adding a range of c' to the properties of the displaced material. We represented c' by a lognormal distribution to provide a higher frequency of low-cohesion values to the model, with the purpose to better represent the unconsolidated nature of sediments at rock glaciers' fronts.
3. Pore pressure was added to the material of configuration 1 by including a normal distribution for r_u.
4. Pore pressure was added to the material of configuration 2 by including a normal distribution for r_u.

For each configuration, we computed the mean factor of safety (FS) and the probability of failure (PF), that is, the fraction of model runs that resulted in a FS < 1.

3.5 | Ground thermal conditions

We inferred pre-failure subsurface conditions at HIN and SIM by analyzing data collected at the nearby LAZ rock glacier (borehole 1). This site is fed by talus from paragneiss and micaschist bedrock. In summer 2010, the active layer in borehole 1 (the one considered in this study) was found to be 2.8 m thick. The active layer and the upper

sections of the permafrost body consist mainly of coarse-grained material with maximum particle diameters of up to 30 cm (Krainer et al., 2015). Ground temperatures (GT) of LAZ at 1, 2, 5, and 15 m depth were compared with T_A (daily values and monthly trend) as well as the modeled SWE at the borehole location. In addition, the autumn and spring zero-curtains were identified. The zero-curtain is defined as the period of constant active layer GT at or slightly below 0°C, which is observed in spring and autumn. This phenomenon occurs due to the release of latent heat generated during the freezing and melting process of water present in the active layer (French, 2007). Hence, an extensive zero-curtain can be indicative for a high moisture content in the active layer (Hoelzle, et al., 2003; Kenner et al., 2019; Zenklusen Mutter & Phillips, 2012).

4 | RESULTS

4.1 | Rock glacier movement

The orthoimage pairs 2006–2008, 2008–2016, and 2016–2019 were used to compute the HIN rock glacier movement, whereas for SIM the orthoimages taken in 2000, 2006, 2008, and 2014 were used. Orthoimages of 2000 and 2014 were not reliable for HIN due to the extensive snow cover, and 2016 and 2019 products were not available for SIM. The minimum detectable displacement rate varied between 1.08 m (SIM, 2006–2008) and 0.39 m (HIN, 2016–2019). The cross validation revealed a linear model to best interpolate movement vectors, providing RMSEs ranging from 0.09 (HIN, 2006–2008) to 0.57 (SIM, 2008–2014). Both rock glacier movement maps show the largest values at the frontal parts of the rock glacier (Figure 3). A movement of 25.6 m over 15 years was found for Zone 2 of SIM.
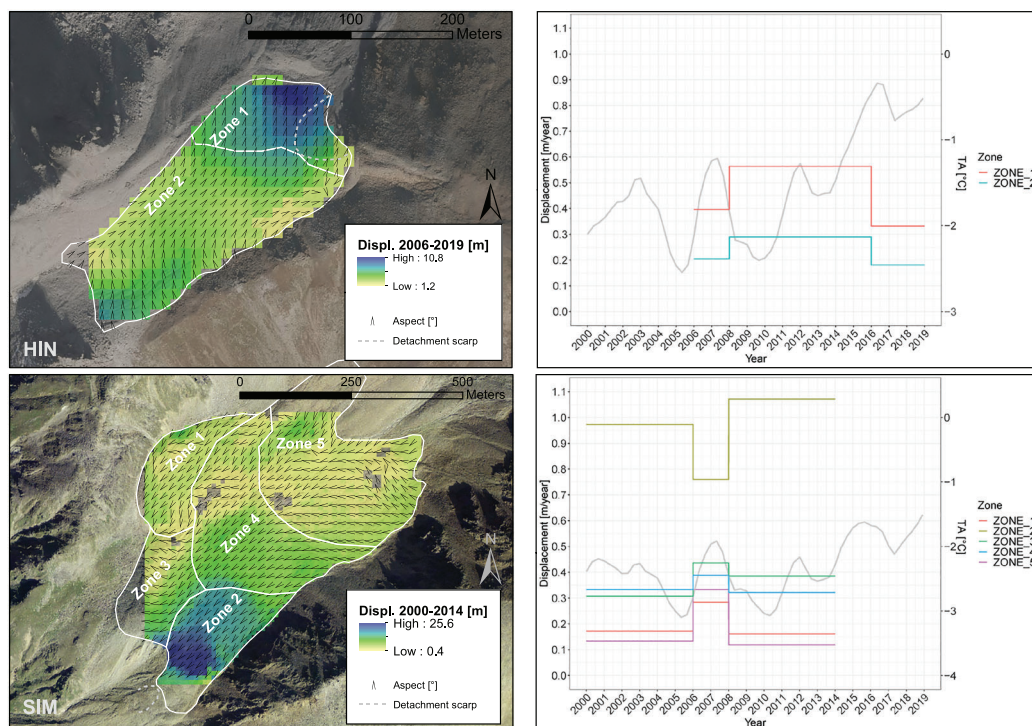

FIGURE 3 Rock glacier surface displacement maps obtained by summing interpolated movement over periods 2000–2006, 2006–2008, and 2008–2014 for SIM (upper left) and 2006–2008, 2008–2016, and 2016–2019 for HIN (lower left). Annual displacement rates in m y^{-1}, and trend component of monthly T_A in °C (gray line, see also Figure 4) are shown in upper and lower right panels. Annual displacement values refer to averaged vectors resulting from the IMCORR analysis. Orthophotos refer to 2008 for SIM and 2016 for HIN

Surface displacement rates decrease nearly concentrically with increasing distance from this "hotspot". Additionally, zone 2 underwent a deceleration phase from 2000 to 2006 to 2006–2008 from nearly 1 m year^{-1} to 0.75 m year^{-1}, whereas the rest of the landform accelerated nearly uniformly. From 2008 on, zone 2 was found to increase flow velocity again to over 1 m year^{-1}, in contrast to the other zones, which slowed down. Analogously, also at HIN the highest displacement rates were found at zone 1, which represents the steeper, frontal part. This part of HIN moved by 10.8 m over 14 years. At HIN rock glacier, both zones accelerated between 2008 and 2016. Then, from 2016 the movement of both parts of the rock glacier decreased, zone 1 to about 0.35 m year^{-1} (Figure 3). In summary, although for both sites no clear temporal trends of annual displacement rates could be observed, their frontal parts showed higher absolute surface displacements over the considered periods with respect to the rest of the landforms.

4.2 | Climate and meteorological parameters

4.2.1 | Climate trends

In contrast to the absence of a clear temporal trend in rock glacier movement pattern, a statistically significant increase in average air temperature (T_A) for the winter, spring, and summer months for Hintergrat and for spring and summer for Similaungrube is statistically detected (Table 2). Instead, no statistically significant change in average precipitation (P) is evident. The positive degree-day sum (PDD) in 2014 was around the long-term average at both sites (i.e., 408°C/64th percentile at HIN and 164°C/42nd percentile at SIM). The cumulated precipitation for the months of June, July, and August (P_{JJA}) was apparently higher in summer 2014 (326 mm/86th percentile at HIN and 353 mm/90th percentile at SIM). In the winter season 2013–2014, SWE_{max} was high on both HIN and SIM. At HIN, hydrological model results show 594 mm (on March 3 2014), which corresponds to the 95th percentile, while at SIM the highest amount of the time series was modeled (787 mm on 4 June 2014). In the winter season 2013–2014, the average melting rate (MLT) was lower at HIN (7.3 mm day^{-1}/32nd percentile of the time series) than at SIM (19.7 mm day^{-1}/84th percentile of the time series). The low MLT at HIN is mainly due to the long period of 75 days between SWE_{max} and SWE_0, which is the longest melt period from 1980 to 2018 (Figure 4).

4.2.2 | Rainfall depth and intensity prior to failure

In addition to the very high cumulative rainfall in summer 2014, high-magnitude precipitation events immediately prior to failure were recorded at the Madritsch and Vernagt rain gauges. The former registered a mean rainfall intensity of 2.9 mm h^{-1} and a rainfall depth of 48.5 mm over a duration of 16.8 h. This event lies above the 95% cumulated frequency of all the storm events since January 2009. Also, this event exceeds the thresholds for debris flow initiation in the provinces of Trentino and South Tyrol proposed by Nikolopoulos et al. (2015) and Marra et al. (2016). At Vernagt, a mean rainfall intensity of 2.3 mm h^{-1} and a rainfall depth of 35.3 mm for 15.3 h were measured. Hence, the event falls slightly below the 95% cumulated frequency again considering all storms since September 2003. However, here the threshold for debris flow initiation by Nikolopoulos et al. (2015) is exceeded, whereas the one by Marra et al. (2016) is not (Figure 5).

4.3 | Geomorphological and geotechnical characteristics

The failure at HIN apparently removed a lateral part of the active layer consisting of pebble-sized clasts embedded in a matrix of fine material. As the exposed ice patch appears to be smooth, without visible signs of rupture, we excluded a failure of the frozen core (Figure 2). The actual thickness of the partially exposed ice core of HIN could not be determined. As visible in Figure 2, the lithology of the surrounding hillslopes of the rock glacier terminus is metamorphic, which confirms that HIN has advanced from the "Ortler" nappe onto the "Campo" basement. Therefore, it is reasonable to assume that the coarse-sized, probably in-situ generated metamorphic sediments adjacent to the rock glacier front might also be present below the finer grained, dolomitic rock glacier material (Figure 6). At SIM, the upper end of the detachment scarp coincides with a spring outlet, which most likely marks the interface between the permafrost table and the partially removed active layer. The outcrop of two ice-debris layers further below is further evidence of the presence of ground ice. Hence, the most likely failure mechanism at SIM was a partial detachment of the active layer along a sliding plane of debris-laden ice. As for HIN, the true extension of the ground ice body is unknown (Figure 6).

The GSD curves of samples taken at the front and lateral slopes indicate a well graded, unconsolidated, and mainly non-cohesive material. The main grain fraction of the front slope material resulted to be coarse to medium gravel for SIM, and fine to medium gravel for HIN. A substantial amount (i.e., 19.3%) of fine material was found in the lateral slope of HIN (Figure 7). We measured friction angles φ of 36.6° (low normal stress σ_N) and 30.9° (high σ_N) for HIN and 38.8° (low σ_N) and 33.0° (high σ_N) for SIM (Figure 8). Figure 6 shows a comparison of the slope angles at the terminal parts of the study objects with the obtained relative maximum φ (i.e., 36.6° for HIN and 38.3°

TABLE 2 Yearly change rate for seasonal aggregates of P and T_A for HIN and SIM obtained by the Theil–Sen estimator and significance level according to the Mann-Kendall test; (*) p < 0.1, (**) p < 0.05, (***) p < 0.01, (–) indicates no significant trend. For a visual comparison of the trends, see Figure 4

Variable	Site	DJF	MAM	JJA	SON
T_A [°C year^{-1}] 1956–2018	HIN	0.007**	0.014***	0.015***	-
	SIM	-	0.009*	0.009***	-
P [mm year^{-1}] 1950–2018	HIN	-	-	-	-
	SIM	-	-	-	-

FIGURE 4 Long-term trends of P, SWE and T_A for HIN and SIM generated by the "STL" algorithm (Cleveland et al., 1990) (a–c). Yearly values of PDD, P_{JJA}, SWE_{max} and MLT for HIN and SIM. X-axis labels of snow-related variables (SWE_{max} and MLT) denotes the second half of winter season (e.g., "1986" refers to the winter season 1985–1986) (d–g). Gray dashed vertical lines indicate failure date 13 August 2014. See Table 2 for Mann-Kendall trend analysis of T_A and P
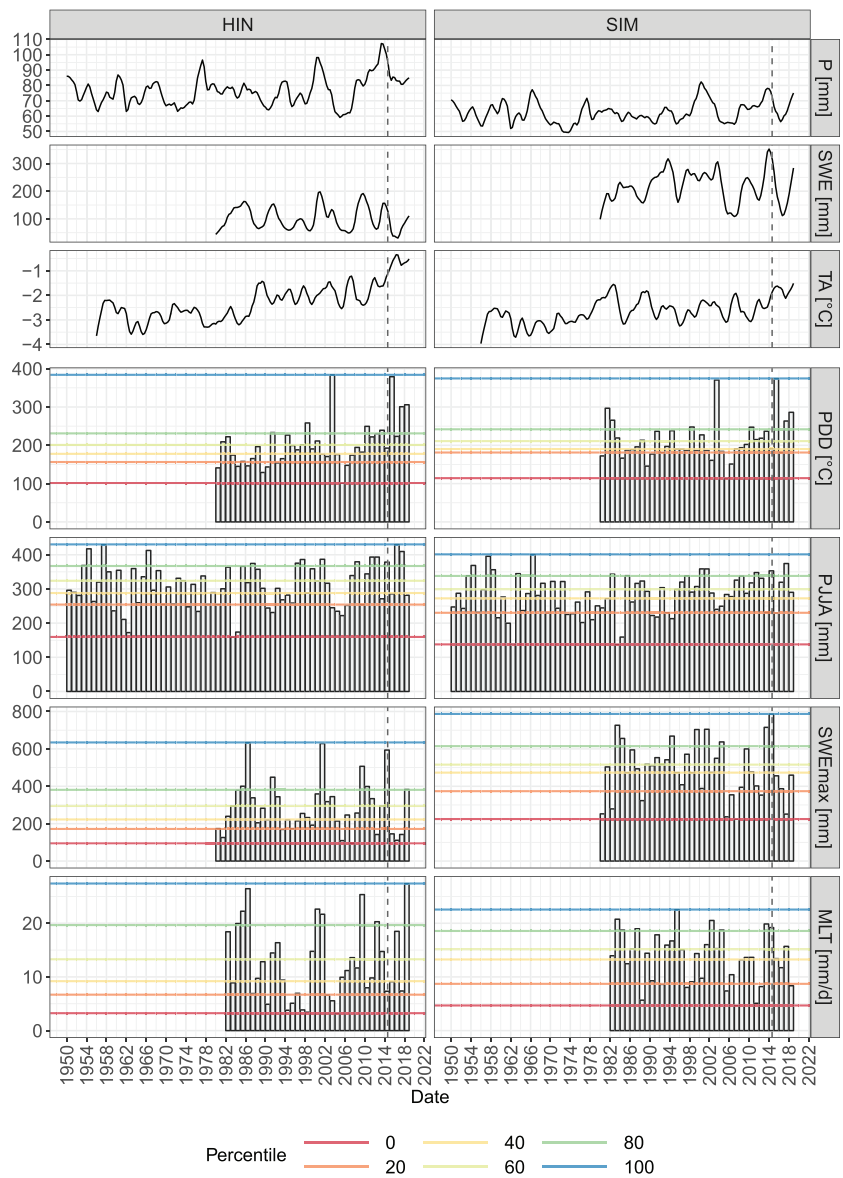

FIGURE 5 ID relationships for Madritsch (MAD) and Vernagt (VER), 50% and 95% cumulated frequency of all registered events and threshold of 5% exceedance probability of summer debris flow initiation for Trentino and South Tyrol of Nikolopoulos et al. (2015) (upper row). ED relationships for MAD and VER, 50% and 95% cumulated frequency of all registered events and threshold of 5% exceedance probability of debris flow initiation for Trentino and South Tyrol of Marra et al. (2016) (lower row). Data refers to period 1 January 2009 to 9 September 2018 (MAD) and 1 August 2003 to 31 December 2018 (VER). Rainfall events related to studied slope failures are highlighted with black circles
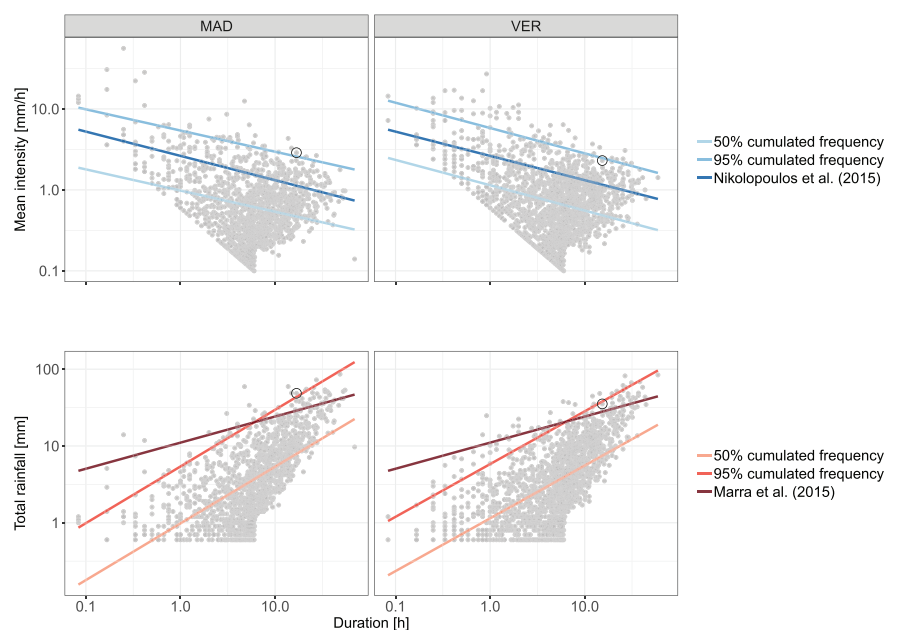
for SIM). The front slope at HIN is generally less steep than φ, except the lateral flank where the failure occurred. SIM in contrast, was characterized by large portions of front slope angles steeper than φ. After the

events, slope inclination in the failure area of both sites corresponded more or less uniformly to φ. The high-slope angles in the post-failure area of SIM indicate the upper and lateral detachment scarps.
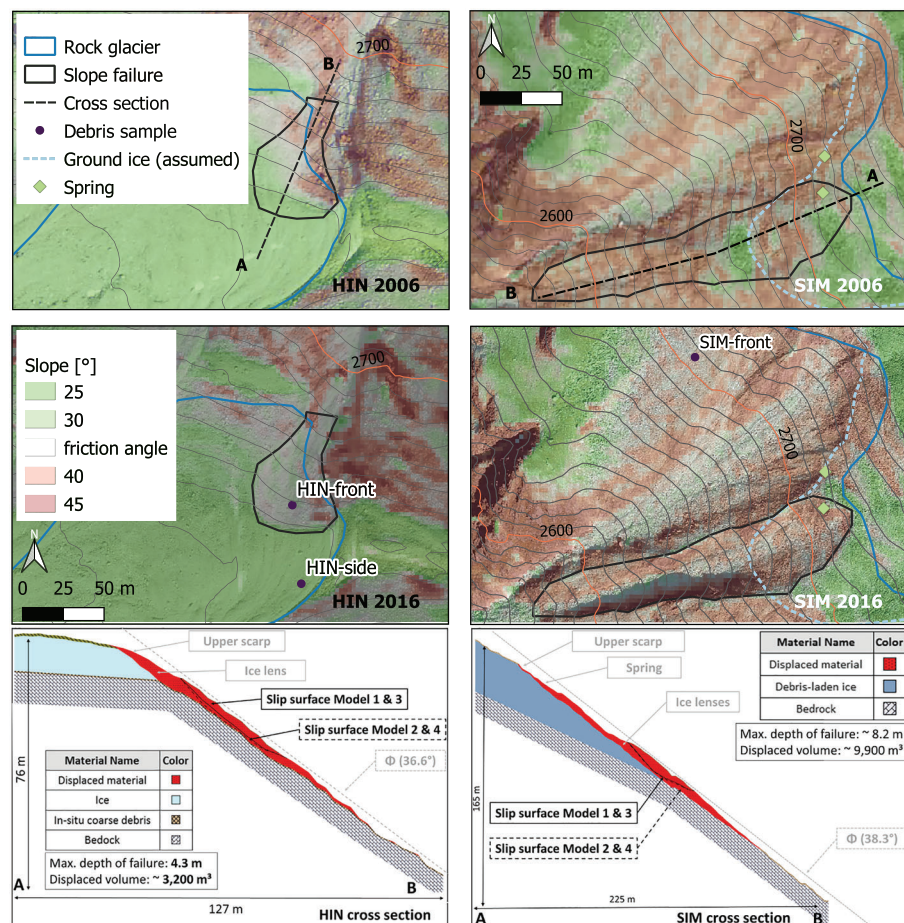
FIGURE 6 Upper two rows: Slope angles of failure area prior and after detachments expressed as distance from measured highest value of φ (i.e., 36.6° for HIN and 38.3° for SIM); equidistance of contour lines is 10 m. Lower row: Two-dimensional model on which slope stability calculations were based on. The red area highlights topographic change prior and after the failure and represents the displaced material. The inclination of the gray dashed line corresponds to the measured highest φ
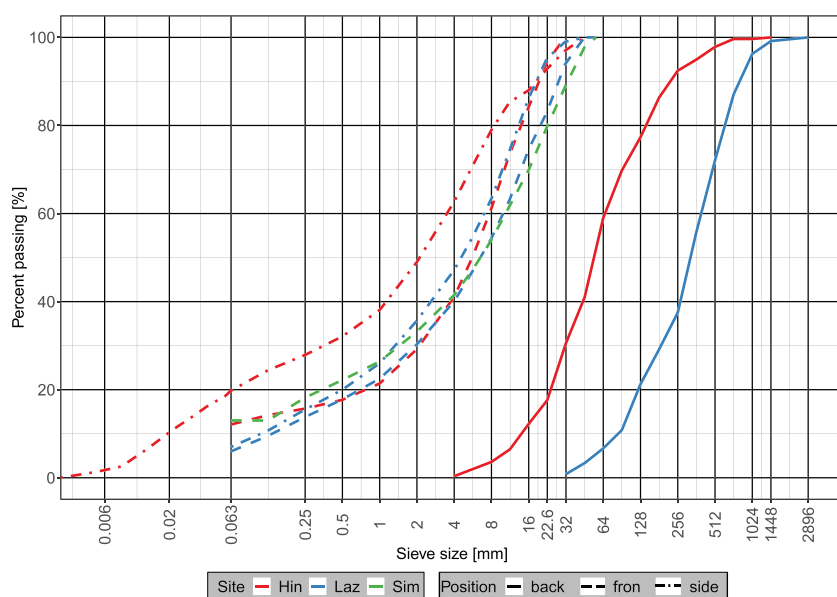

FIGURE 7 Grain size distribution (GSD) curves of the samples taken at HIN, SIM, and LAZ

Direct shear tests resulted in c' equal to 14.9 kPa (low σ_N) and 19.1 kPa (high σ_N) for SIM, and 0 kPa (low σ_N) and 23.1 kPa (high σ_N) for HIN (Figure 8). This latter value is surprisingly high considering the grain size distribution of the material. However, we attribute the high c' values not to the properties of the sampled material but to the geotechnical testing procedure. Our samples were tested under the Mohr-Coulomb assumption of linearity between shear strength τ_f and normal stress σ_N, where tan(φ) defines the slope and c' the y-axis intercept of the fitted linear function. However, it is known that this relationship might be also non-linear and tends to overestimate slope

stability due to a too high c' (e.g., Charles & Soares, 1984). Consequently, the parameter range for geotechnical modeling was further constrained by additionally considering literature values of geotechnical parameters measured for rock glaciers, moraines and talus slopes (Figure 8). Maximum φ obtained by direct shear testing was set as mean and literature values defined the parameter range. Values for c' were instead entirely assigned based on literature values (Figure 8, Table 3).

The first modeling configuration resulted shows marginally stable conditions for the HIN rock glacier, with mean FS = 1.00 and PF = 50.6%. PF equals 100% below 36°, and gradually decreases

FIGURE 8 Geotechnical testing results compared with literature values of φ and c' obtained by direct shear tests on moraines (M), rock glaciers (RG) and scree slopes (SS). Testing results of the present study are highlighted with black circles. All values refer to φ and c' obtained by considering peak shear stress. ([†]) test results of Arnold et al. (2005) with a density index I_D = 0.4 are shown; ([‡]) Lucas et al. (2020) used triaxial shear testing; ([§]) average values of the tested geological units by Opsal (2017) are shown; ([¶]) Springman et al. (2003) conducted direct shear tests under partially saturated condition
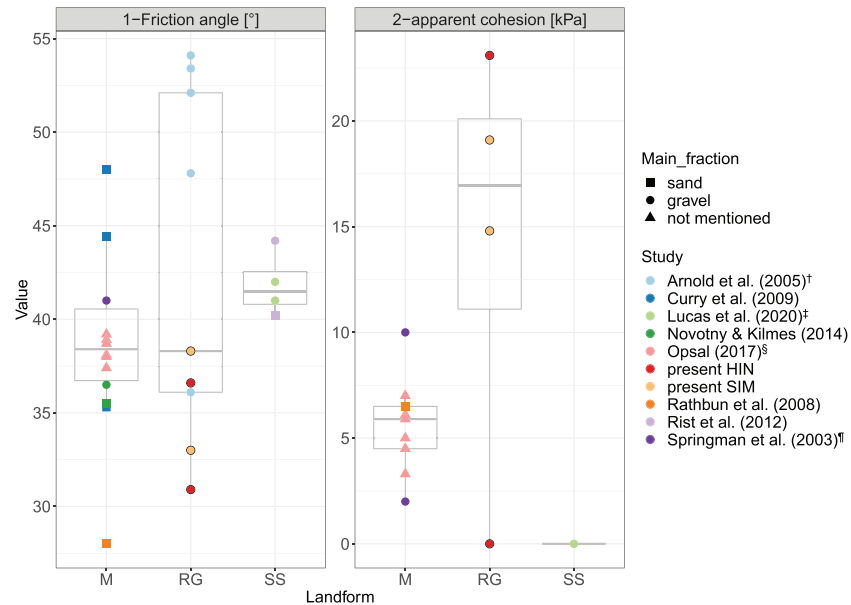

TABLE 3 Input parameter range for geotechnical modeling

Parameter	Distribution	Site	Mean (μ)	Standard deviation (σ)	Value range
Φ [°]	Normal	HIN	36.6	3	28–54.1
		SIM	38.3	3	28–54.1
c' [kPa]	Lognormal	HIN	3	1	0–10
		SIM	3	1	0–10
r_u [−]	Normal	HIN	0.15	0.05	0–0.3
		SIM	0.15	0.05	0–0.3

between 36° and 38°. For the SIM rock glacier, the first configuration resulted in more stable conditions, with PF = 100% only if φ is < 34° (i.e., FS = 1.14 and PF of 11.5%) (Table 4, Figure 9). The second model simulations led to a stabilization of HIN with a mean FS = 1.16 and a PF = 8.7%. Already a c' = 1.5 kPa caused a decrease of PF to by 20%. The stabilizing effect of c' was found to be even more pronounced at SIM, where the mean FS rose to 1.23 and PF dropped to 1.2%. Over the entire range of c', no substantially high PF was obtained. Adding pore pressure to the model led to a remarkable destabilization of both slopes (model configuration 3); the mean FS of HIN dropped to 0.76 and PF rose to 96.5%. PF did not lower significantly for the whole range of φ. Also for SIM, the presence of pore pressure resulted in a FS < 1; a φ beyond 42° would lower FS by around 20%. The fourth model setup including φ, c' and r_u resulted in a mean FS for HIN = 0.92 and an overall PF = 75.7%. Already at a r_u between 0.08 and 0.1 PF is > 50%. The last simulation provides overall unstable conditions also for SIM, with FS = 0.97 and PF = 62.6%. However, PF over the range of r_u is generally lower compared to HIN (Table 4, Figure 9). In summary, geotechnical investigations suggest a more failure-prone material for HIN, where particle cohesion may have provided additional strength. SIM was found to be characterized by a coarser material with a higher friction angle allowing for a steeper slope setting.

4.4 | Ground thermal conditions

The 2014 hydrological year (i.e., 1 October 2013 to 30 September 2014) was characterized by a high cumulative snow amount, long

TABLE 4 Probability of failure (PF) and mean factor of safety (FS) for modeling configurations 1–4 for HIN and SIM

Site	HIN		SIM	
Model configuration	FS	PF	FS	PF
1	1.00	50.9%	1.14	11.5%
2	1.16	8.7%	1.23	1.2%
3	0.76	96.5%	0.89	81.0%
4	0.92	75.7%	0.97	62.6%

lasting zero curtains (i.e., 97 days in autumn and 53 days in spring) and moderate ground temperatures (GT). In comparison, minimum GT in 2012 were much lower, together with a thinner snow cover and a shorter spring zero curtain (i.e., 42 days). The autumn zero curtain for 2012 could not be determined due to an interruption of GT measurements between 23 June 2011 and 13 March 2012 (Figure 10, Table 5).

5 | DISCUSSION

5.1 | Triggers of the rock glacier front failures and their regional context

The studied rock glacier front slope failures occurred in response to precipitation events on 13 August 2014. Both rainfall depth-duration (ED) and intensity-duration (ID) analysis revealed these events to be around the 95% cumulated frequency of all the rainfall events
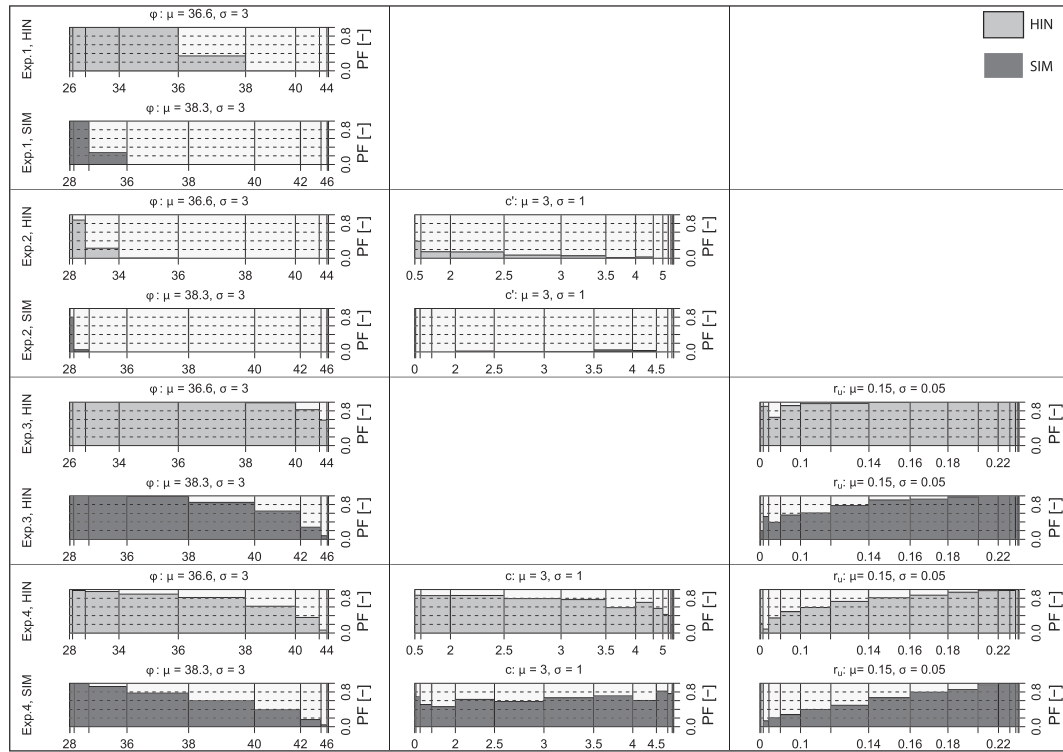
FIGURE 9 Failure probability (PF) of HIN (light-gray shaded bars) and SIM (dark-gray shaded bars) of the four modeling experiments plotted over the range of model parameters (Table 3). Row-pairs refer to modeling experiments 1–4 for HIN and SIM, columns to the model parameters φ, c' and r_u. Mean μ and standard deviation σ are given in header of each plot
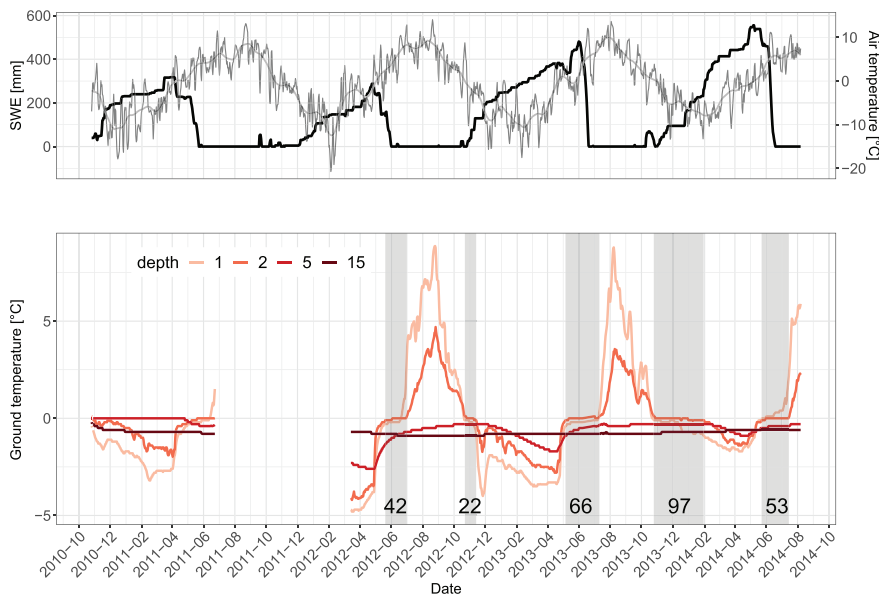

FIGURE 10 Upper panel: SWE (black line), daily and 30-day running mean of T_A (dark gray line and light gray line, respectively); lower panel: GT measured in borehole 1 of LAZ at 1, 2, 5, and 15 m depth. The gray-shaded areas show spring and autumn zero-curtains at 2 m depth and the black numbers within show duration in days of the zero-curtains

recorded in the period 2009–2018 and 2003–2018 at the available rain gauges of Madritsch and Vernagt, respectively (Figure 5). Our findings are in line with Kummert et al. (2017), who identified infrequently high amounts of rainfall as triggers for retrogressive erosion on rock glacier fronts in the Swiss Mattertal. The clear "tipping" role of low-frequency, high-magnitude rainfall events contrasts to the findings by Marcer et al. (2020), who identified many small- and medium-intensity rather than one high-intensity rainfall event as the cause of the Lou rock glacier slope failure (Table 6).

Several additional natural hazard events were registered on 13 August 2014. It is remarkable that a large portion of debris flows and debris floods occurred in high-elevation catchments (i.e., Sulden

Valley, Schnals Valley and Ridnaun/Ridanna Valley), and for quite a few of them a direct glacial or periglacial origin was identified (cf. section 2.3, Figure 1). We argue that this points out the role of destabilizing preparatory factors which have affected the frozen ground at these sites. Indeed, the high number of registered events over a large area also shows that the strong precipitation was not a local anomaly.

5.2 | Preparation of slope failures

In the context of the investigated rock glacier front failures, air temperature might not have been a major driving force as average values

TABLE 5 SWE$_{max}$, length of snow cover period, minimum GT (GT$_{min}$), and zero curtain length obtained for LAZ for hydrological years that were covered by borehole measurements

Hydrological year (01.10–30.09)	SWE$_{max}$ [mm]	Snow cover period	GT$_{min}$ [°C]	Zero curtain duration [d]		Zero curtain period	
				Autumn	Spring	Autumn	Spring
2011–2012	304.5	Nov. 7 - May 30	−4.2	-	42	-	May 20–July 1
2012–2013	524.9	Oct. 26 - June 20	−2.8	22	66	Oct. 22 - Nov. 13	May 6–July 11
2013–2014	592.3	Oct. 10 - June 18	−1.4	97	53	Oct. 25 - Jan. 30	May 23–July 15

for the positive degree-day sum in 2014 have shown. Moderate temperatures in 2014 were not surprising since cumulated precipitation for the summer months revealed June, July, and August 2014 to be exceptionally wet. The maximum snow water equivalent (SWE) values in the hydrological year of 2014 were among the highest over the entire time series of 1980–2018, which indicated an important role of snow melting and snow cover (Figure 4, Table 2). Again, our findings are congruent with results of Kummert et al. (2017), who identified phases of intense snow melting as drivers for erosion occurring at rock glacier fronts (Table 6). In analogy to the abundant SWE, ground temperatures in the borehole of the Lazaun (LAZ) rock glacier were higher compared with the previous winter seasons (Figure 10). For comparison, GT in the winter season 2011–2012 was low, and we attribute this fact to the late and thin snow cover that has enabled a throughout cooling of the active layer. The spring zero-curtain in 2012 then was shorter than in the following years due to the reduced melting period of snow and the lower input of melt water. Then, during the winter season 2013–2014, an opposite situation to 2011–2012 was observed, as the insulating effect of the abundant snow cover apparently led to higher ground temperatures (Table 5). Finally, the 2014 melting season initiated under moist ground conditions. The melting of the extensive snowpack as well as the abnormally abundant spring and summer rainfalls have likely shifted the rock glacier slopes even closer to their marginal stability. Melt rate, if any, played a role only on SIM, while on HIN the snow cover decreased over a relatively long period, which can be explained by the average values of T$_A$ in 2014 (Figure 4). Marcer et al. (2020) again reported a contrary situation preceding the front slope failures at the Lou rock glacier in August 2015. There, a snow-poor winter followed by a heat wave between mid-June and mid-July were thought to have favored a substantial ground warming.

Atmospheric temperatures control the thermal regime of rock glaciers through heat conduction (Cicoira et al., 2019a; Haeberli et al., 2006). Consequently, permafrost temperatures within HIN and SIM probably have risen as the trend of a multiannual increase of T$_A$ during spring and summer months suggests. This further implies an overall rising presence of liquid water within the permafrost in the rock glaciers. The consequences are a further intensification of permafrost warming by advection of heat as well higher pore pressures in the shear horizon and therefore an increase in flow velocity (Cicoira et al., 2019b; Delaloye et al., 2013; Luethi et al., 2017). Measured surface displacement rates of our study objects however were in the order of 0.1–1 m year^{-1}, which is in line with data measured on other rock glaciers that were not found destabilized (e.g., Bodin et al., 2018; Fey & Krainer, 2020).

The available series of orthophotos was not long enough to detect a trend in surface displacement rate. Long-term rock glacier monitoring initiatives however confirm a clear increase of their flow velocities. (cf. PERMOS, 2019). At both HIN and SIM, horizontal displacement rates at the rock glacier terminus were high compared to other parts of the landforms. This indicates a high sediment transfer rate towards the rock glacier fronts and their adjacent debris slopes, that is, depositional areas of loose sediment that can be mobilized later (cf. Kummert et al., 2017). The observed speed-up of the frontal zone of HIN and SIM indicates an influence of rock glacier creep on the predisposition of their marginal areas for rapid mass movements. However, the temporal resolution of our analysis was too coarse to establish a reliable causal relationship with the slope failures. Additionally, the measured surface displacement rates are deemed to underestimate the actual progression of the steeper parts (e.g., the rock glacier front) as the image correlation method did not account for vertical changes (Figure 3).

5.3 | Predisposing factors

The predisposition for failure of both slopes was essentially driven by local topographic and sedimentary conditions. In fact, HIN and SIM are connected in terms of sediment fluxes to their respective downstream channel (Figure 2). This connection has been enabling the removal of sediments at the rock glacier front and thus prevented the creation of a stabilizing, buttressing layer of coarse debris at their toes. The stability of the investigated rock glacier snouts therefore was provided only by the geotechnical properties of the fine-grained front slope material. The first modeling experiment has shown that HIN is marginally stable if φ corresponds approximately to the slope angle. The same experiment resulted in a substantially lower failure probability (PF) of SIM, indicating that φ alone can provide a reasonable degree of stability. The fact that slope portions of HIN and SIM were found to be steeper than the measured φ might stem from several reasons (Figure 9). Firstly, the size of our geotechnical samples was rather small, and some slope portions may have a higher φ than what we have measured. Secondly, it is reasonable to assume that a complete absence of c' was not the case. Studies conducted on steep, partially saturated moraine slopes—with a comparable GSD—showed that negative, suction-driven pore pressure could increase soil apparent cohesion and therefore its shear strength (Springman et al., 2003; Teysseire, 2006). Indeed, the second modeling configuration for HIN shows that little values for c' (i.e., 1.5 kPa) may lower PF substantially (Figure 9, Table 4). As the third modeling simulations did not consider c', this might be the most representative of the real conditions occurred during the failure, as suction-derived cohesive strength disappears once soil approach saturation. The high

TABLE 6 Comparison of the present work with selected studies about rock glaciers affected by front slope instabilities; (†) inferred by us based on published images; (‡) inferred from electrical resistivity tomography (ERT) and seismic refraction (SRT)

Site		Hintergrat (I)	Similaungrube (I)	Dirru (CH)	Gugla (CH)	Tsarmine (CH)	Ritigraben (CH)	Lou (F)
Failure type		Active layer failure	Active layer failure	Erosion	Erosion	Erosion	Erosion, active layer failure	Linear regressive erosion, active layer detachment
Process type		Debris flow	Debris flow	Rock fall, debris slide, superficial and concentrated flow	Rock fall, debris slide, superficial and concentrated flow	Rock fall, debris slide, superficial and concentrated flow	Debris flow	Debris flow
Frequency of events		Isolated events	Isolated events	Continuous low magnitude vents, occasional high magnitude events (concentrated flow)	Continuous low magnitude vents, occasional high magnitude events (concentrated flow)	Continuous low magnitude vents, occasional high magnitude events (concentrated flow)	Occasional debris flows	Isolated events
Predisposition	Altitude	2,700	2,750	2,530	2,620	2,460	2,550	2,800
	Exposure	NE	SW	W	W	W	W	N
	Surface and subsurface composition	- Pebbly surface layer embedded in fine matrix - Presumably clean ice underneath	- Bouldery surface layer - Presumably debris-laden ice	- Bouldery† - Fine grained at front - Presumably high interstitial ice content	- Bouldery† - Three superimposed shear horizons - Probably low ice content	- Openwork boulders - Shear horizon 15 m below front line - High ice content excluded	- Coarse blocky - Ice-rich - Temperate, water-rich permafrost - Talik at ca. 12 m depth	- Pebbly surface layer - Ice content varying from massive to low‡
Preparatory	Displacement rate [m year^{-1}]	0.1 - 1	0.1 - 1	1 - 10	1 - 10	1 - 10	0.1 - 10	0.1 - 10
	Antecedent snow conditions	- Thick snow cover - High SWE	- Thick snow cover - High SWE	- Intense snow melt - Heavy or repeated rainfall§	- Intense snow melt - Heavy or repeated rainfall§	- Intense snow melt - Heavy or repeated rainfall§		Thin snow cover
	Antecedent atmospheric conditions	- Average T_A - High cumulative rainfall	- Average T_A - High cumulative rainfall				Warm and wet summers	Drought period
Triggering rainfall		Low frequency – high magnitude	Low frequency – high magnitude				- Advective and convective rainfall - Rain-on-snow	High frequency – low magnitude
Reference		present work	present work	Kummert et al., 2017; Kummert & Delaloye, 2018	Kummert et al., 2017; Kummert & Delaloye, 2018	Kummert et al., 2017; Kummert & Delaloye, 2018	Kenner et al., 2017; Lueth et al., 2017; Lugon & Stoffel, 2010	Marcer et al., 2020

sensitivity of the model relative to the pore pressure coefficient r_u can be explained by the nature of this parameter; as shown in modeling simulation 1, the ratio between shear strength and stress results in a FS close to 1 or slightly above. Adding a fraction of the vertical stress induced by the weight of the soil column as pore pressure to shear strength, results in its reduction and consequently lowers FS.

Previous studies showed that rock glacier discharge follows mainly seasonal pattern of snow melt and rainfall, while only a little fraction of it is provided by permafrost ice melting (e.g., Krainer et al., 2015; Krainer & Mostler, 2000; Wagner et al., 2020). Hence, topography and composition of the catchments draining to the study rock glaciers were assumed to play an important role in controlling the slope failures (cf. Groh & Blöthe, 2019). In contrast to SIM, the relatively small, elongated catchment area for HIN is considered to be unfavorable with respect to the delivery of runoff, snow and sediments to the rock glacier (Figure 1, Table 1). We argue that the relatively fine-grained sediment composition at HIN plays an important role as it brings about a slower dissipation of pore pressures due to a reduced seepage through the sediment layer. In contrast, a nearly immediate dissipation of pore pressures may be assumed in the coarser grained SIM front, where its open-work surface may lead to very high infiltration rates. For both sites it may be reasonable to assume that the presence of an impermeable ice layer has favored rapid water concentration near the rock glacier front (Figure 6). Therefore, the failure at SIM might have originated near the ice-debris outcrop, on which water runoff is visible in Figure 2. A similar failure mechanism was reported recently by Marcer et al. (2020) concerning the failure of the eastern frontal part of the Lou rock glacier.

5.4 | A word of caution on the inclusion of Lazaun borehole data

We included Lazaun in our study with the aim to gain insight into ground thermal and hydrological conditions of our study objects prior to failure. Subsurface conditions in high mountain environments however may be very heterogeneous also within small spatial distances, which hinders a simple comparison between sites (cf. Rist & Phillips, 2005; Schmid et al., 2012; Wagner et al., 2019). Consequently, a comparison of external environmental properties between LAZ and the study objects was undertaken to infer on their subsurface conditions. The borehole II of LAZ is located at 2,538 m a.s.l. with "permafrost mostly in cold conditions," according to the Alpine Permafrost Index Map (APIM) of Boeckli et al. (2012a, 2012b). Cold conditions on LAZ are mainly assured by a reduced incoming direct solar radiation due to its northeastern orientation and the cirque-shaped surrounding topography as well as its coarse blocky surface composition, which is known to favor lower GT through cooling effects (Gorbunov et al., 2004; Gruber & Hoelzle, 2008; Hoelzle et al., 2003; Juliussen & Humlum, 2008). The frontal part of SIM is located approximately 200 m higher than LAZ but is oriented towards southeast. Similarly to LAZ, APIM suggests "permafrost mostly in cold conditions," which for SIM are provided by a similar coarse openwork surface composition than LAZ, as aerial photographs suggest. In summary, a comparison of topographical and sediment characteristics suggests GT conditions of SIM being

similar to LAZ. The frontal part of HIN is substantially higher than borehole II of LAZ (ca. 200 m) and the rock glacier is northeast-exposed. Not surprisingly, APIM suggests "permafrost in nearly all conditions" for this site. Given the more favorable topographic setting for permafrost presence, a lower GT compared with LAZ was expected, although the surface and surface-near structure of HIN is dominated by fine-grained sediment, which indicates an absence of cooling effects observed on coarse blocky surfaces.

6 | CONCLUSIONS

The slope stability analysis for Hintergrat (HIN) confirmed a marginal stability of the rock glacier front slope if shear strength was provided only by friction angle. However, the substantial amount of fine material in the sample taken at the lateral slope of HIN, slope portions steeper than the measured angle of internal friction as well as probabilistic modeling results suggest the presence of an additional strength component, e.g., apparent cohesion in unsaturated material. In contrast, the front slope of Similaungrube (SIM) was composed of coarser sediment and consequently had a higher friction angle, and particle cohesion is not necessary to provide stability. The triggering event at both rock glaciers was a high-intensity rainstorm, estimated to be around the 95th percentile of all the recorded storms over the last 15 (Vernagt) and 11 (Madritsch) years. The fact that no or only minor previous or subsequent failure events were registered at both sites indicates that even more intensive rainstorms did not result in a slope failure (assuming that the event catalog is complete for the studied sites). We therefore conclude that the sedimentary properties and the triggering rainfall event alone cannot explain the occurrence of the slope failures. Consequently, hypothesis 1 is rejected.

The simultaneous occurrence of several other events on 13 August 2014 originating in glacial or periglacial areas let us assume a prominent role of ice melting in high-altitude slopes besides the ones under investigation. Hence, the involvement of destabilizing factors acting on a timescale beyond the short-term trigger was considered as very likely. Our data suggests that destabilization is to be expected if medium-term antecedent conditions are characterized by snow-rich and rainy conditions. The abundant 2013–2014 winter snowpack and the abnormally wet spring and summer in 2014 have probably thickened and saturated the active layer of both rock glaciers. The high-magnitude rainfall event was then the tipping point towards slope failure. Hence, hypothesis 2 cannot be rejected.

Air temperature was found to have increased significantly from the 1950s onwards during the spring and summer months. A subsequent increased presence of liquid water within the rock glaciers, as well as their topographic setting, may explain their higher movement at the marginal slopes. Unfortunately, the coarse temporal resolution of the movement analysis did not allow us to obtain accurate indications on the effect of rock glacier creep on the investigated slope failures. Thereferore, Hypothesis 3 could not be properly tested and thus cannot be reliably rejected. However, a connection to raising atmospheric temperatures is probable as rock glacier creep rates have increased in the last decades over the entire European Alpine arc (e.g., Kellerer-Pirklbauer et al., 2018).

Finally, it is worth mentioning how additional data on the internal structure and thermal conditions of the two studied rock glaciers

would have been desirable, rather than using a different site nearby to derive such information. Unfortunately, there are only very few instrumented rock glaciers throughout the Alps, and our study highlights the extreme value of such monitoring activities, also in light of mitigation towards mountain geohazards.

CONFLICTS OF INTEREST

The authors declare no conflicts of interest.

DATA AVAILABILITY STATEMENT

Data can be made available upon request to the corresponding author.

ORCID

Christian Kofler https://orcid.org/0000-0002-1634-7645
Stephan Gruber https://orcid.org/0000-0002-1079-1542
Stefan Steger https://orcid.org/0000-0003-0886-5191
Marc Zebisch https://orcid.org/0000-0002-3530-7219
Stefan Schneiderbauer https://orcid.org/0000-0001-7587-849X
Francesco Comiti https://orcid.org/0000-0001-9840-0165

REFERENCES

Arenson, L.U. & Springman, S.M. (2005) Mathematical descriptions for the behaviour of ice-rich frozen soils at temperatures close to 0 °C. *Canadian Geotechnical Journal*, 42(2), 431–442. https://doi.org/10.1139/t04-109

Arnold, A., Thielen, A. & Springman, S.M. (2005) On the stability of active layers in alpine permafrost. In: Senneset, K. (Ed.) *Landslides and Avalanches: ICFL 2005 Norway. Presented at the 11th Interantional Conference and Field Trip on Landslides*. Norway: Taylor & Francis Group.

Avian, M., Kellerer-Pirklbauer, A. & Bauer, A. (2009) LiDAR for monitoring mass movements in permafrost environments at the cirque Hinteres Langtal, Austria, between 2000 and 2008. *Natural Hazards and Earth System Sciences*, 9(4), 1087–1094. https://doi.org/10.5194/nhess-9-1087-2009

Barsch, D. (1996) *Rockglaciers - Indicators for the Present and Former Geoecology in High Mountain Environments, Springer Series in Physical Environment*. Berlin Heidelberg, Heidelberg: Springer.

Bernstein, R. (1983) Image geometry and rectification. In: Colwell, R.N. (Ed.) *Manual of Remote Sensing*. Falls Church, VA: American Society of Photogrammetry, pp. 881–884.

Berthling, I. (2011) Beyond confusion: Rock glaciers as cryo-conditioned landforms. *Geomorphology*, 131(3–4), 98–106. https://doi.org/10.1016/j.geomorph.2011.05.002

Bishop, A.W. (1955) The use of the Slip Circle in the Stability Analysis of Slopes. *Géotechnique*, 5(1), 7–17. https://doi.org/10.1680/geot.1955.5.1.7

Bishop, A.W. & Morgenstern, N. (1960) Stability Coefficients for Earth Slopes. *Géotechnique*, 10(4), 129–153. https://doi.org/10.1680/geot.1960.10.4.129

Bodin, X., Krysiecki, J.-M., Schoeneich, P., Le Roux, O., Lorier, L., Echelard, T. *et al.* (2017) The 2006 Collapse of the Bérard Rock Glacier (Southern French Alps): The 2006's Collapse of the Bérard Rock Glacier. *Permafrost and Periglacial Processes*, 28(1), 209–223. https://doi.org/10.1002/ppp.1887

Bodin, X., Thibert, E., Sanchez, O., Rabatel, A. & Jaillet, S. (2018) Multi-Annual Kinematics of an Active Rock Glacier Quantified from Very High-Resolution DEMs: An Application-Case in the French Alps. *Remote Sensing*, 10, 15.

Boeckli, L., Brenning, A., Gruber, S. & Noetzli, J. (2012a) A statistical approach to modelling permafrost distribution in the European Alps or similar mountain ranges. *The Cryosphere*, 6(1), 125–140. https://doi.org/10.5194/tc-6-125-2012

Boeckli, L., Brenning, A., Gruber, S. & Noetzli, J. (2012b) Permafrost distribution in the European Alps: calculation and evaluation of an index map and summary statistics. *The Cryosphere*, 6(4), 807–820. https://doi.org/10.5194/tc-6-807-2012

Bollmann, E., Rieg, L., Spross, M., Sailer, R., Bucher, K., Maukisch, M. *et al.* (2012) Blockgletscherkataster in Südtirol - Erstellung und Analyse. In: Sailer, R. (Ed.) *Permafrost in Südtirol*. Innsbruck, Austria: Innsbrucker Geographische Studien. University of Innsbruck, pp. 147–171.

Brenning, A. (2008) Statistical geocomputing combining R and SAGA: The example of landslide susceptibility analysis with generalized additive models. *Hamburger Beiträge Zur Physischen Geographie Und Landschaftsökologie*, 19, 23–32.

Brunetti, M.T., Peruccacci, S., Rossi, M., Luciani, S., Valigi, D. & Guzzetti, F. (2010) Rainfall thresholds for the possible occurrence of landslides in Italy. *Natural Hazards and Earth System Sciences*, 10(3), 447–458. https://doi.org/10.5194/nhess-10-447-2010

Buchli, T., Kos, A., Limpach, P., Merz, K., Zhou, X. & Springman, S.M. (2018) Kinematic investigations on the Furggwanghorn Rock Glacier, Switzerland. *Permafrost and Periglacial Processes*, 29(1), 3–20. https://doi.org/10.1002/ppp.1968

Bunte, K. & Abt, S.R. (2001) *Sampling surface and subsurface particle-size distributions in wadable gravel-and cobble-bed streams for analyses in sediment transport, hydraulics, and streamed monitoring (Technical Report No. RMRS-GTR-74)*. Fort Collins, CO: U.S. Department of Agriculture, Forest Service, Rocky Mountain Research Station.

Charles, J.A. & Soares, M.M. (1984) The stability of slopes in soils with nonlinear failure envelopes. *Canadian Geotechnical Journal*, 21(3), 397–406. https://doi.org/10.1139/t84-044

Cicoira, A., Beutel, J., Faillettaz, J. & Vieli, A. (2019b) Water controls the seasonal rhythm of rock glacier flow. *Earth and Planetary Science Letters*, 528, 115844. https://doi.org/10.1016/j.epsl.2019.115844

Cicoira, A., Beutel, J., Faillettaz, J., Gärtner-Roer, I. & Vieli, A. (2019a) Resolving the influence of temperature forcing through heat conduction on rock glacier dynamics: a numerical modelling approach. *The Cryosphere*, 16, 927–942.

Conrad, O., Bechtel, B., Bock, M., Dietrich, H., Fischer, E., Gerlitz, L. *et al.* (2015) System for Automated Geoscientific Analyses (SAGA) v. 2.1.4. *Geoscientific Model Development*, 8, 1991–2007. https://doi.org/10.5194/gmd-8-1991-2015

Crespi, A., Matiu, M., Bertoldi, G., Petitta, M. & Zebisch, M. (2021) A high-resolution gridded dataset of daily temperature and precipitation records (1980–2018) for Trentino – South Tyrol (north-eastern Italian Alps). *Earth System System Science Data Discussions*. https://doi.org/10.5194/essd-2020-346

Curry, A.M., Sands, T.B. & Porter, P.R. (2009) Geotechnical controls on a steep lateral moraine undergoing paraglacial slope adjustment. In: Harrison, S. & Knight, J. (Eds.) *Periglacial and Paraglacial Processes and Environments, Geological Society, London*. London, UK: Special Publications. Geological Society, pp. 181–197.

Delaloye, R., Lambiel, C. & Gärtner-Roer, I. (2010) Overview of rock glacier kinematics research in the Swiss Alps. *Geographica Helvetica*, 65(2), 135–145. https://doi.org/10.5194/gh-65-135-2010

Delaloye, R., Morard, S., Barboux, C., Abbet, D., Gruber, V., Riedo, M. & Gachet, S. (2013) Rapidly moving rock glaciers in Mattertal. In: *Publikation Zur Jahrestagung Der Schweizerischen Geomorphologischen Gesellschaft*. Switzerland: St. Niklaus, pp. 21–31.

El-Ramly, H., Morgenstern, N.R. & Cruden, D.M. (2005) Probabilistic assessment of stability of a cut slope in residual soil. *Géotechnique*, 55(1), 77–84. https://doi.org/10.1680/geot.2005.55.1.77

Fey, C. & Krainer, K. (2020) Analyses of UAV and GNSS based flow velocity variations of the rock glacier Lazaun (Ötztal Alps, South Tyrol, Italy). *Geomorphology*, 365, 107261. https://doi.org/10.1016/j.geomorph.2020.107261

Formetta, G., Kampf, S.K., David, O. & Rigon, R. (2014) Snow water equivalent modeling components in NewAge-JGrass. *Geoscientific Model Development*, 7(3), 725–736. https://doi.org/10.5194/gmd-7-725-2014

Formetta, G., Mantilla, R., Franceschi, S., Antonello, A. & Rigon, R. (2011) The JGrass-NewAge system for forecasting and managing the hydrological budgets at the basin scale: models of flow generation and propagation/routing. *Geoscientific Model Development*, 4(4), 943–955. https://doi.org/10.5194/gmd-4-943-2011

French, H.M. (2007) *The periglacial environment*, Third edition. Hoboken, New Jersey, USA: Wiley and Sons, Ltd.

GAPHAZ. (2017) Assessment of Glacier and Permafrost Hazards in Mountain Regions - Technical Guidance Document. Prepared by Allen, S., Frey, H., Huggel, C. et al. Standing Group on Glacier and Permafrost Hazards in Mountains (GAPHAZ) of the International Association of Cryospheric Sciences (IACS) and the International Permafrost Association (IPA). Zurich, Switzerland / Lima, Peru, 72 pp.

Glade, T. & Crozier, M.J. (2005) The Nature of Landslide Hazard Impact. In: Glade, T., Anderson, M. & Crozier, M.J. (Eds.) *Landslide Hazard and Risk*. Chichester, West Sussex, UK: John Wiley & Sons, Ltd, pp. 43–74.

Gorbunov, A.P., Marchenko, S.S. & Seversky, E.V. (2004) The thermal environment of blocky materials in the mountains of Central Asia. *Permafrost and Periglacial Processes*, 15(1), 95–98. https://doi.org/10.1002/ppp.478

Groh, T. & Blöthe, J.H. (2019) Rock Glacier Kinematics in the Kaunertal, Ötztal Alps, Austria. *Geosciences*, 9(9), 373. https://doi.org/10.3390/geosciences9090373

Gruber, S., Fleiner, R., Guegan, E., Prajjwal, P., Schmid, M.-O., Stumm, D. et al. (2017) Review article: Inferring permafrost and permafrost thaw in the mountains of the Hindu Kush Himalaya region. *The Cryosphere*, 11(1), 81–99. https://doi.org/10.5194/tc-11-81-2017

Gruber, S. & Hoelzle, M. (2008) The cooling effect of coarse blocks revisited: a modeling study of a purely conductive mechanism. In: *9th International Conference on Permafrost. Fairbanks, Alaska*. Fairbanks, Alaska: Institute of Northern Engineering University of Alaska Fairbanks, pp. 557–561.

Haeberli, W., Hallet, B., Arenson, L., Elconin, R., Humlum, O., Kääb, A. et al. (2006) Permafrost creep and rock glacier dynamics. *Permafrost and Periglacial Processes*, 17(3), 189–214. https://doi.org/10.1002/ppp.561

Haeberli, W., Hoelzle, M., Kääb, A., Keller, F., Vonder Mühl, D.V. & Wagner, S. (1998) Ten years after drilling through the permafrostof the active rock glacier Murtèl, Eastern Swiss Alps: Answered questions and new perspectives. In: *Proceedings of the 7th International Conference on Permafrost*. Canada: Yellowknife, p. 8.

Hartl, L., Fischer, A., Stocker-waldhuber, M. & Abermann, J. (2016) Recent speed-up of an alpine rock glacier: an updated chronology of the kinematics of outer hochebenkar rock glacier based on geodetic measurements. *Geografiska Annaler: Series a, Physical Geography*, 98(2), 129–141. https://doi.org/10.1111/geoa.12127

Hock, R., Rasul, G., Adler, C., Cáceres, S., Gruber, S., Hirabayashi, Y. et al. (2019) High Mountain Areas. In: Pörtner, H.-O., Roberts, D.C., Masson-Delmotte, V., Zhai, P., Tignor, M., Poloczanska, E. et al. (Eds.) *IPCC Special Report on the Ocean and Cryosphere in a Changing Climate*. In press.

Hoelzle, M., Haeberli, W. & Stocker-Mittaz, C. (2003) Miniature ground temperature data logger measurements 2000–2002 in the Murtèl-Corvatsch area, Eastern Swiss Alps. In: Phillips, M., Springman, S. & Arenson, L. (Eds.) *Proceedings of the 8th International Conference on Permafrost*. Lisse, Zürich, Switzerland: Swets & Zeitlinger, p. 7.

IPCC. (2019) Summary for Policymakers. In: Pörtner, H.-O., Roberts, D., Masson-Delmotte, V., Zhai, P., Tignor, M., Poloczanska, E. et al. (Eds.) *IPCC Special Report on the Ocean and Cryosphere in a Changing Climate*. In press.

Jones, D.B., Harrison, S., Anderson, K. & Betts, R.A. (2018) Mountain rock glaciers contain globally significant water stores. *Scientific Reports*, 8(1), 2834. https://doi.org/10.1038/s41598-018-21244-w

Juliussen, H. & Humlum, O. (2008) Thermal regime of openwork block fields on the mountains Elgåhogna and Sølen, central-eastern Norway. *Permafrost and Periglacial Processes*, 19(1), 1–18. https://doi.org/10.1002/ppp.607

Kellerer-Pirklbauer, A., Delaloye, R., Lambiel, C., Gärtner-Roer, I., Kaufmann, V., Scapozza, C. et al. (2018) Interannual variability of rock glacier flow velocities in the European Alps. In: Book of Abstracts. Presented at the 5th European Conference On Permafrost, p. 3.

Kendall, M.G. (1957) Rank correlation methods. *Econometrica*, 25, 181–183.

Kenner, R., Phillips, M., Beutel, J., Hiller, M., Limpach, P., Pointner, E. & Volken, M. (2017) Factors Controlling Velocity Variations at Short-Term, Seasonal and Multiyear Time Scales, Ritigraben Rock Glacier, Western Swiss Alps: Factors driving rock glacier velocity at three time scales. *Permafrost and Periglacial Processes*, 28(4), 675–684. https://doi.org/10.1002/ppp.1953

Kenner, R., Pruessner, L., Beutel, J., Limpach, P. & Phillips, M. (2019) How rock glacier hydrology, deformation velocities and ground temperatures interact: Examples from the Swiss Alps. *Permafrost and Periglac Process*, 31(1), 3–14. https://doi.org/10.1002/ppp.2023

Kofler, C., Steger, S., Mair, V., Zebisch, M., Comiti, F. & Schneiderbauer, S. (2020) An inventory-driven rock glacier status model (intact vs. relict) for South Tyrol, Eastern Italian Alps. *Geomorphology*, 350, 106887. https://doi.org/10.1016/j.geomorph.2019.106887

Krainer, K., Bressan, D., Dietre, B., Haas, J.N., Hajdas, I., Lang, K. et al. (2015) A 10,300-year-old permafrost core from the active rock glacier Lazaun, southern Ötztal Alps (South Tyrol, northern Italy). *Quaternary Research*, 83(2), 324–335. https://doi.org/10.1016/j.yqres.2014.12.005

Krainer, K. & Mostler, W. (2000) Reichenkar rock glacier: a glacier derived debris-ice system in the western Stubai Alps, Austria. *Permafrost and Periglacial Processes*, 11(3), 267–275. https://doi.org/10.1002/1099-1530(200007/09)11:3%3C267::AID-PPP350%3E3.0.CO;2-E

Krainer, K., Mussner, L., Behm, M. & Hausmann, H. (2012) Multi-disciplinary investigation of an active rock glacier in the Sella Group (Dolomites, Northern Italy). *Austrian Journal of Earth Sciences*, 105, 48–62.

Kummert, M. & Delaloye, R. (2018) Mapping and quantifying sediment transfer between the front of rapidly moving rock glaciers and torrential gullies. *Geomorphology*, 309, 60–76. https://doi.org/10.1016/j.geomorph.2018.02.021

Kummert, M., Delaloye, R. & Braillard, L. (2017) Erosion and sediment transfer processes at the front of rapidly moving rock glaciers: Systematic observations with automatic cameras in the western Swiss Alps. *Permafrost and Periglacial Processes*, 29(1), 21–33. https://doi.org/10.1002/ppp.1960

Lacasse, S., Liu, Z. & Nadim, F. (2017) *Probabilistic Characterization of Soil Properties—Recognition of Wilson Tang's Contribution to Geotechnical*

Practice, in: Geotechnical Safety and Reliability. Presented at the Geo-Risk 2017. Denver, Colorado: American Society of Civil Engineers, pp. 2–26.

Lucas, D., Fankhauser, K., Maurer, H., McArdell, B., Grob, R., Herzog, R. et al. (2020) Slope Stability of a Scree Slope Based on Integrated Characterisation and Monitoring. Water, 12(2), 447. https://doi.org/10.3390/w12020447

Luethi, R., Phillips, M. & Lehning, M. (2017) Estimating Non-Conductive Heat Flow Leading to Intra-Permafrost Talik Formation at the Ritigraben Rock Glacier (Western Swiss Alps): Estimating non-Conductive Heat Flow. Permafrost and Periglacial Processes, 28(1), 183–194. https://doi.org/10.1002/ppp.1911

Lugon, R. & Stoffel, M. (2010) Rock-glacier dynamics and magnitude–frequency relations of debris flows in a high-elevation watershed: Ritigraben, Swiss Alps. Global and Planetary Change, 73(3–4), 202–210. https://doi.org/10.1016/j.gloplacha.2010.06.004

Mair, V., Nocker, C. & Tropper, P. (2007) Das Ortler-Campo Kristallin in Südtirol. Mitteilungen der Österreichischen Mineralogischen Gesellschaft, 153, 219–240.

Mann, H.B. (1945) Nonparametric tests against trend. Econometrica, 13(3), 245–259. https://doi.org/10.2307/1907187

Marcer, M., Ringsø Nielsen, S., Ribeyre, C., Kummert, M., Duvillard, P., Schoeneich, P. et al. (2020) Investigating the slope failures at the Lou rock glacier front, French Alps. Permafrost and Periglac Process, 31(1), 15–30. https://doi.org/10.1002/ppp.2035

Marra, F., Nikolopoulos, E.I., Creutin, J.D. & Borga, M. (2016) Space–time organization of debris flows-triggering rainfall and its effect on the identification of the rainfall threshold relationship. Journal of Hydrology, Flash Floods, Hydro-Geomorphic Response and Risk Management, 541, 246–255. https://doi.org/10.1016/j.jhydrol.2015.10.010

Nadim, F. (2007) Tools and strategies for dealing with uncertainty in geotechnics. In: Griffiths, D.V. & Fenton, G. (Eds.) Probabilistic Methods in Geotechnical Engineering, International Center for Mechanical Sciences. Wien New York: Springer Wien New York. https://doi.org/10.1007/978-3-211-73366-0_2

Nikolopoulos, E.I., Borga, M., Marra, F., Crema, S. & Marchi, L. (2015) Debris flows in the eastern Italian Alps: Seasonality and atmospheric circulation patterns. Natural Hazards and Earth System Science, 15(3), 647–656. https://doi.org/10.5194/nhess-15-647-2015

Opsal, Ø.L. (2017) Shear strength of dry tills from the southern half of Norway in relation to bedrock geology. NJG, 97(2), 145–169. https://doi.org/10.17850/njg97-2-04

PERMOS. (2019) Permafrost in Switzerland 2014/2015 to 2017/2018.

R Core Team. (2017) R: A language and environment for statistical computing. Vienna, Austria: R Foundation for Statistical Computing.

Rathbun, A.P., Marone, C., Alley, R.B. & Anandakrishnan, S. (2008) Laboratory study of the frictional rheology of sheared till. Journal of Geophysical Research: Earth Surface, 113(F2). https://doi.org/10.1029/2007JF000815

Rist, A. & Phillips, M. (2005) First results of investigations on hydrothermal processes within the active layer above alpine permafrost in steep terrain. Norsk Geografisk Tidsskrift - Norwegian Journal of Geography, 59(2), 177–183. https://doi.org/10.1080/00291950510020574

Rocscience. (2019) Slide2. Toronto, Canada: Rocscience.

Schlögel, R., Kofler, C., Gariano, S.L., Campenhout, J.V. & Plummer, S. (2020) Changes in climate patterns and their association to natural hazard distribution in South Tyrol (Eastern Italian Alps). Scientific Reports, 10(1), 1–14. https://doi.org/10.1038/s41598-020-61615-w

Schmid, M.-O., Gubler, S., Fiddes, J. & Gruber, S. (2012) Inferring snowpack ripening and melt-out from distributed measurements of near-surface ground temperatures. The Cryosphere, 6(5), 1127–1139. https://doi.org/10.5194/tc-6-1127-2012

Scotti, R., Crosta, G.B. & Villa, A. (2017) Destabilisation of Creeping Permafrost: The Plator Rock Glacier Case Study (Central Italian Alps).

Permafrost and Periglacial Processes, 28(1), 224–236. https://doi.org/10.1002/ppp.1917

Sen, P.K. (1968) Estimates of the regression coefficient based on Kendall's tau. Journal of the American Statistical Association, 63(324), 1379–1389. https://doi.org/10.2307/2285891

Springman, S.M., Arenson, L.U., Yamamoto, Y., Maurer, H., Kos, A., Buchli, T. & Derungs, G. (2012) Multidisciplinary investigations on three rock glaciers in the Swiss Alps: Legacies and future perspectives. Geografiska Annaler: Series a, Physical Geography, 94(2), 215–243. https://doi.org/10.1111/j.1468-0459.2012.00464.x

Springman, S.M., Jommi, C. & Teysseire, P. (2003) Instabilities on moraine slopes induced by loss of suction: a case history. Géotechnique, 53(1), 3–10. https://doi.org/10.1680/geot.2003.53.1.3

Steger, S. (2017) Spatial analysis and statistical modelling of landslide susceptibility – pitfalls and solutions (Doctoral Thesis). Vienna, Austria: University of Vienna.

Stingl, V. & Mair, V. (2005) Einführung in die Geologie Südtirols. Bozen/Bolzano: Autonome Provinz Bozen - Südtirol.

Tang, W. (1984) Principles of probabilistic characterization of soil properties. In: Probabilistic Characterization of Soil Properties: Bridge Between Theory and Practice. ASCE, pp. 4–89.

Teysseire, P. (2006) Geotechnische Eigenschaften von Moränen (Doctoral Thesis). ETH Zurich, Zürich, Switzerland. https://doi.org/10.3929/ETHZ-A-005166289

Theil, H. (1950) A rank-invariant method of linear and polynomial regression analysis. I, II, III. In: Proceedings of the Koninklijke Nederlandse Akademie Wetenschappen, Series A Mathematical Sciences. pp. 386–392, 521–525, 1397–1412.

Thies, H., Nickus, U., Tolotti, M., Tessadri, R. & Krainer, K. (2013) Evidence of rock glacier melt impacts on water chemistry and diatoms in high mountain streams. Cold Regions Science and Technology, 96, 77–85. https://doi.org/10.1016/j.coldregions.2013.06.006

Vivero, S. & Lambiel, C. (2019) Monitoring the crisis of a rock glacier with repeated UAV surveys. Geographica Helvetica, 74(1), 59–69. https://doi.org/10.5194/gh-74-59-2019

Wagner, T., Brodacz, A., Krainer, K. & Winkler, G. (2020) Active rock glaciers as shallow groundwater reservoirs, Austrian Alps. Grundwasser - Zeitschrift der Fachsektion Hydrogeologie, 25(3), 215–230. https://doi.org/10.1007/s00767-020-00455-x

Wagner, T., Pauritsch, M., Mayaud, C., Kellerer-Pirklbauer, A., Thalheim, F. & Winkler, G. (2019) Controlling factors of microclimate in blocky surface layers of two nearby relict rock glaciers (Niedere Tauern Range, Austria). Geografiska Annaler: Series A, Physical Geography, 101(4), 1–24. https://doi.org/10.1080/04353676.2019.1670950

Zenklusen Mutter, E. & Phillips, M. (2012) Active Layer Characteristics At Ten Borehole Sites In Alpine Permafrost Terrain, Switzerland: Active Layer Development in Alpine Permafrost Terrain. Permafrost and Periglacial Processes, 23(2), 138–151. https://doi.org/10.1002/ppp.1738

Zhang, J., Tang, W.H. & Zhang, L.M. (2010) Efficient Probabilistic Back-Analysis of Slope Stability Model Parameters. Journal of Geotechnical and Geoenviromental Engineering, 136(1), 99–109. https://doi.org/10.1061/(ASCE)GT.1943-5606.0000205

SUPPORTING INFORMATION

Additional supporting information may be found online in the Supporting Information section at the end of this article.